Excitation with quantum light. I. Exciting a harmonic oscillator

J. C. López Carreño[1] and F. P. Laussy[2,1]

[1]*Departamento de Física Teórica de la Materia Condensada, Universidad Autónoma de Madrid, 28049 Madrid, Spain*
[2]*Russian Quantum Center, Novaya 100, 143025 Skolkovo, Moscow Region, Russia*

We present a two-part study of the excitation of an optical target by quantum light. In this first part, we introduce the problematic and address the first case of interest, that of exciting the quantum harmonic oscillator, corresponding to, e.g., a single-mode passive cavity or a noninteracting bosonic field. We introduce a mapping of the Hilbert space that allows to chart usefully the accessible regions. We then consider the quantum excitation from single-photon sources in the form of a two-level system under various regimes of (classical) pumping: incoherent, coherent, and in the Mollow triplet regime. We close this first part with an overview of the material to be covered in the subsequent work.

I. INTRODUCTION

Photonics [1] has been highly successful in the engineering of quantum sources since the proof-of-principle production of quantum light in the mid-1970s [2,3]. Befitting its status of the elementary brick of the light field, the single photon was the first type of genuinely nonclassical type of light and gave rise to the concept of a single-photon source (SPS) [4–6]. Nowadays, SPS abound with ever increasing figures of merit [7–11] and are even commercially available. The motivations for SPS are many [12], from metrology [13,14] to input for quantum information processing [15–17], passing by biotechnology [18,19], sensing and detecting [20,21], etc. In most cases, the technology is still under development and quantum light is not yet deployed on the market. For this reason, the focus is still largely on the source itself rather than on its direct use as part of a technological component. There is, however, an increasing interest in using quantum light for actual applications. For instance, there have been recently converging propositions from independent groups to use quantum light for spectroscopy [22–26].

Thanks to the theory of frequency-resolved photon correlations [27], it was shown how quantum sources can be greatly tuned in their characteristics by selecting light in astute frequency windows, revealed by the theory in the form of so-called "two-photon correlations spectra" [28,29]. This can be used to identify and exploit unsuspected types of quantum correlations [30] and/or enhance them by learned combination of time scales and frequencies [31], merely by spectral filtering of a quantum emitter [32]. Beyond optimizing parameters to find the best compromises for sought applications, the theory also reveals that interesting quantum signal is typically not found at the expected spectral locations such as peaks, that correspond to classical-like deexcitation of the emitter between real states at the one-photon level. Instead, strong quantum correlations arise from, e.g., two-photon deexcitation involving intermediate virtual states. Such channels of deexcitation were termed "*leapfrog processes*" [28,29]. They are emitted in unremarkable frequency windows at the photoluminescence level. At the quantum-optical level, however, they are the quintessence of quantum emission. This picture has been confirmed experimentally by Müller's group [33]. A closer look at, and proper selection of, the photons emitted by quantum sources thus appears fundamental

for state-of-the-art quantum applications, their correlations being otherwise averaged over often competing types. This viewpoint of frequency-resolved photon correlations therefore poses in a new light the problem of the excitation of optical targets with such inside knowledge of the features of the sources. This revives a question put to close scrutiny by Gardiner [34] and Carmichael [35] in 1993 following the emergence of sources of squeezed light [36], which appeared sufficiently more elaborate as compared to SPS to warrant a direct investigation of how they would affect optical targets as compared to conventional types of excitation (classical fields, possibly stochastic). Resonance fluorescence in the squeezed vacuum has in fact been just recently reported [37]. Gardiner and Carmichael's (independent) treatment of the problem of quantum excitation in two consecutive papers in the Physical Review [34,35] achieved the setting up of a formalism, named the "*cascaded formalism*" by Carmichael, that allows to excite a system (which we will call the "target") by another (the "source") without back-action from the target to the source. This permits to think separately of the quantum source, whose properties can be first studied (through the two-photon spectrum, for instance) and then directed onto a target. For historical accuracy, let us mention that the problem was first contemplated by Kolobov and Sokolov [38] who tackled it by providing all the correlations of the exciting quantum field. This was recognized as an overkill by Gardiner and Carmichael [34,35] (Gardiner had made prior attempts along these lines). They proposed instead to model the quantum source dynamics as well as the response of the target, even if only the latter is of interest. From our point of view, such a treatment is essential since the frequency correlations of the source are too complicated to be treated otherwise than fully and explicitly by solving the complete problem. Also, such correlations are dynamical in character, and cannot be well approximated by quantum states as initial conditions. Instead, they must be dealt with through the full apparatus of dissipative quantum optics, feeding the target with the complete treatment of virtual states and other types of strongly correlated quantum input. The cascaded formalism is therefore particularly apposite for exciting optical systems with the knowledge of the two-photon correlation spectrum of an emitter.

Despite the conceptual importance of quantum excitation, there has been a moderate followup of this cascaded formalism,

which we believe is a deep and far-reaching contribution to the problem of light-matter interaction. Even though it became textbook material (see the last chapter from one of the pioneering authors [39]) and generated a sizable amount of citations, few texts do actually fully exploit the idea. Gardiner and Parkins (the formalism is sometimes also named after these two authors) undertook a more thorough analysis of various types of nonstandard statistics of the source [40] and Cirac *et al.* used it to describe perfect transmission in their proposal for a quantum network [41], but overall, the core of the literature using the formalism focuses on specialized particular cases, such as driving with squeezed light [42,43]. Typically, the discussion is then held at the level of correlations from a quantum state (namely, a squeezed state), as opposed to dynamical correlations from a quantum source. The other studies, already evoked, turned to approximate or indirect approaches, quite similar to the earlier attempts before the cascaded formalism was set up. The reasons for this are certainly a mix between convenience of using well-known and established formalism and the as-yet unclear advantages of the alternative one.

In this and subsequent work, we make an extensive study of exciting with quantum light (with no feedback from the target to the source), and show that some new features of light-matter interaction emerge, making the overall problem in need of scrupulous attention. The formalism itself needs little further development and we will mainly adapt it to new cases but with the additional knowledge provided by frequency-resolved correlations (we will extend the formalism in the following papers to consider sequences of cascades and multiple sources). We briefly introduce its core machinery in a self-contained way in Sec. II as a convenience for the reader, and refer to the original works for details of the derivation [34,35] or to the Supplemental Material of Ref. [26], where it is cast in the problematic of the present text. Section III gives an overview of the many possibilities one can study as well as details of the configurations we focus on in future work. After what can be seen as a long introduction, Sec. IV introduces the first important results by providing a way to characterize quantum states of the harmonic oscillator in a space of quantum-optical diagonal correlators, which will be helpful to later characterize the sources, and with effect to disprove a popular criterion for single-photon states. Sections V and VI characterize the incoherent and coherent SPS, respectively. As the latter will prove to be more interesting, we devote most of our attention to this case. Section VII shows that the advantages of the cascaded coupling over the conventional Hamiltonian coupling (cavity QED) remain present even when considering alternative descriptions of coupling between the source and the target. Section VIII draws the conclusions for the cases studied here, while Sec. IX does so for the wider picture of cascaded coupling and introduces the other cases to be investigated in followup papers.

II. THEORETICAL BACKGROUND

The coupling between two quantum systems is typically given by an interaction Hamiltonian. In the second quantization formalism, such a Hamiltonian reads in its most simple form (we take $\hbar = 1$ along the paper):

$$H_I = g(c_1^\dagger c_2 + c_2^\dagger c_1), \quad (1)$$

where c_1, c_2 are annihilation operators describing the particles of the coupled system, and g is their interaction strength. If the particles described by c_i have a decay rate γ_i, and are freely evolving with a Hamiltonian H_i, $i = 1,2$, the master equation describing the dynamics of this system is:

$$\partial_t \rho = i[\rho, H_1 + H_2 + H_I] + \frac{\gamma_1}{2}\mathcal{L}_{c_1}\rho + \frac{\gamma_2}{2}\mathcal{L}_{c_2}\rho, \quad (2)$$

where $\mathcal{L}_c \rho = (2c\rho c^\dagger - c^\dagger c \rho - \rho c^\dagger c)$. Depending on whether the coupling H_I or the dissipation γ_i dominates, one speaks of strong or weak coupling, respectively. If one of the two systems, say, 1, is itself excited externally, for instance being driven by a laser, or merely being given a nonvacuum initial condition, then one has a crude picture of system 1 exciting system 2. This is a fairly accurate description in the weak-coupling limit where the dynamics seems irreversible, simply because excitations are dissipated before they can cycle back (we discuss in Sec. VII when this becomes exact).

The coupling between quantum systems does not have to be reversible: it can instead correspond to the scenario of a source and its target. In this case, there is a deep asymmetry between the coupled systems. For instance, one can remove the target from the beam of the source, which leaves the latter unaffected while the former passes from being irradiated to the vacuum. Note that such an asymmetry does not have to hold on logical grounds. In fact, in electronics, while an ideal source should not be affected by the circuit it powers, in reality, there is a load and every component affects all the others to some extent. In photonics, the picture of a flying qubit, left to propagate long enough before it meets its target, makes it intuitively clear that it should be possible to forbid back-action. This could also be realized by taking advantage of the fast-growing field of chiral optics [45–52]. Theoretically, this asymmetry is achieved by the cascaded coupling [39], where the equations of motion are expressed in the quantum Langevin form, thus allowing to set the output field of one of the systems (the source) as the input field for the other (the target). This can be brought to a master-equation type of description, with both coherent and Lindblad terms that contrive to direct the flow of excitation from the source to target only. This makes all the operators of the source independent from those of the target, while in turn those depend on operators of the source. The generic case where the source (resp. target) is described by the Hamiltonian H_1 (resp. H_2) and has a decay rate γ_1 (resp. γ_2) is ruled by the following master equation [39]:

$$\partial_t \rho = i[\rho, H_1 + H_2] + \frac{\gamma_1}{2}\mathcal{L}_{c_1}\rho + \frac{\gamma_2}{2}\mathcal{L}_{c_2}\rho$$
$$- \sqrt{\gamma_1 \gamma_2}([c_2^\dagger, c_1 \rho] + [\rho c_1^\dagger, c_2]). \quad (3)$$

The source must also be excited, which can be done either by an incoherent or by a coherent type of (classical) excitation. The incoherent excitation is described simply by adding the Lindblad term $(P_{c_1}/2)\mathcal{L}_{c_1^\dagger}\rho$ to Eq. (3). The coherent excitation, however, requires a subtler description, for which one uses the input-output formalism. The coupling between a coherent field and the system (the latter will be used as the source

of quantum excitation) happens through an input channel for said system. If such an input channel is the only one available to excite the source, then it follows that the only output channel from the source also contains the coherence of the driving field. In this case, the target of the quantum excitation is *also* driven by the coherent field, and its dynamics is given by Eq. (3) setting $H_1 = \omega_1 c_1^\dagger c_1 - i\sqrt{\gamma_1}\mathcal{E}(c_1^\dagger - c_1)$, and $H_2 = \omega_2 c_2^\dagger c_2 - i\sqrt{\gamma_2}\mathcal{E}(c_2^\dagger - c_2)$, i.e., the dynamics is ruled by the master equation:

$$\partial_t \rho = i[\rho, \omega_1 c_1^\dagger c_1 + \omega_2 c_2^\dagger c_2 - i\sqrt{\gamma_1}\mathcal{E}(c_1^\dagger - c_1)$$
$$- i\sqrt{\gamma_2}\mathcal{E}(c_2^\dagger - c_2)] + \frac{\gamma_1}{2}\mathcal{L}_{c_1}\rho + \frac{\gamma_2}{2}\mathcal{L}_{c_2}\rho$$
$$- \sqrt{\gamma_1\gamma_2}([c_2^\dagger, c_1\rho] + [\rho c_1^\dagger, c_2]), \quad (4)$$

where $\mathcal{E}$ is the amplitude of the coherent field driving the source. Note that the effective driving intensity, i.e., $\Omega_1 = \sqrt{\gamma_1}\mathcal{E}$, depends on the decay rate of the system that is being excited, in agreement with the fact that a system that cannot emit cannot be excited either. To prevent the target to be also driven by the coherent field, one can use other input (and their corresponding output) channels to excite the source (and also the target). Each of these channels couples to the source with an amplitude $\epsilon_i \leqslant 1$, with the condition that $\sum_k \epsilon_k = 1$, the sum being over all the input channels. In this case, and considering only two input channels (with amplitudes ϵ_1 and $\epsilon_2 = 1 - \epsilon_1$) as well as only one input channel for the target (with amplitude 1), the dynamics of the system is given by Eq. (3) with $H_1 = \omega_1 c_1^\dagger c_1 - i\sqrt{\epsilon_1\gamma_1}\mathcal{E}(c_1^\dagger - c_1)$, $H_2 = \omega_2 c_2^\dagger c_2$, and replacing the coupling strength $\sqrt{\gamma_1\gamma_2}$ by $\sqrt{(1-\epsilon_1)\gamma_1\gamma_2}$ in the second line of Eq. (3), i.e., the dynamics is now ruled by the master equation:

$$\partial_t \rho = i[\rho, \omega_1 c_1^\dagger c_1 + \omega_2 c_2^\dagger c_2 - i\sqrt{\epsilon_1\gamma_1}\mathcal{E}(c_1^\dagger - c_1)] + \frac{\gamma_1}{2}\mathcal{L}_{c_1}\rho$$
$$+ \frac{\gamma_2}{2}\mathcal{L}_{c_2}\rho - \sqrt{\epsilon_2\gamma_1\gamma_2}([c_2^\dagger, c_1\rho] + [\rho c_1^\dagger, c_2]), \quad (5)$$

where $\epsilon_2 = 1 - \epsilon_1$. The additional input channel to the source makes the coupling between the coherent field not as efficient as when there is only one input channel, thus reducing the effective driving intensity. For the target, although the coupling strength is also reduced, now the driving is uniquely due to the emission from the quantum source.

Putting Eq. (3) in the Lindblad form contributes a Hamiltonian part. The formalism thus corresponds to a quantum coherent coupling, allowing the description of continuous wave (cw) and resonant excitation of quantum states. Importantly, in contrast to the Hamiltonian coupling in Eq. (1), the coupling strength is now fixed by the decay rates of the source and of the target. An infinitely lived target cannot be excited. The stronger one wishes to make the coupling between a source and its target, the stronger has to be their (geometric) mean dissipation. This imposes some fundamental constraints on external driving (or driving without feedback). In contrast, Hamiltonian coupling sets the coupling strength and decay rates independently. While it would therefore appear that the Hamiltonian coupling has the upper hand, and that one should strive for the standard strong-coupling regime, we will show

in the following that the cascaded architecture can be superior to the other types of coupling in some cases.

III. QUANTUM SOURCES AND OPTICAL TARGETS

The general problem of excitation with quantum light has obviously numerous ramifications. To the already large variety of optical targets, one now has to combine a much enlarged set of quantum sources. This literally opens a new dimension to optics. Indeed, classical excitation could arguably be limited to a rather small set of categories:

(a) incoherent excitation [incoherent pumping, Boltzmann dynamics, thermal baths, equilibrium, etc., cf. Fig. 1(a)]

(b) coherent excitation [driving with a laser, cf. Fig. 1(b)]; (we postpone to future work the discussion of time-dependent and pulsed excitation and consider until then the case of continuous wave excitation, cf. Sec. IX). Quantum light, on the other hand, encompasses not only the above (if only because
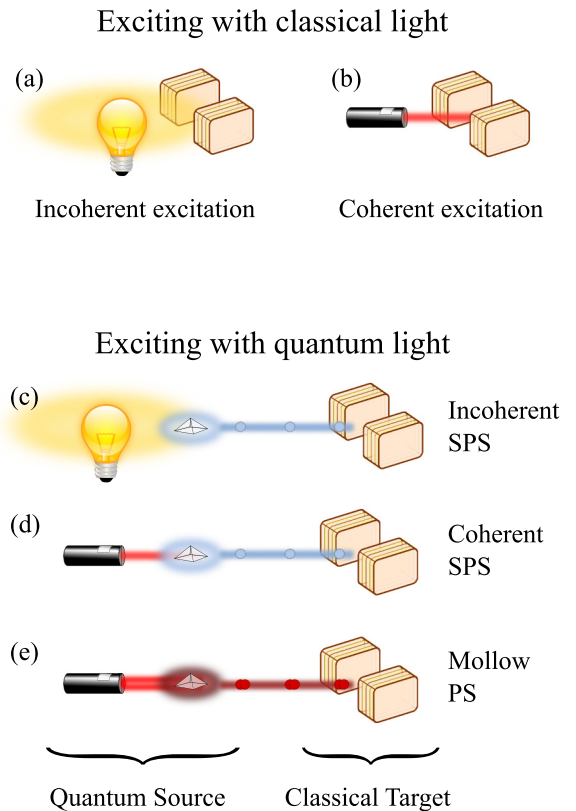

FIG. 1. Upper part: the two main types of classical excitation. The harmonic oscillator can be implemented by a single-mode cavity, sketched here as two distributed Bragg reflectors facing each other. The SPS can be implemented by a quantum dot, sketched here as a little pyramid, as it would be grown by self-assembly [44]. (a) Incoherent excitation, typically corresponding to thermal light. (b) Coherent excitation, typically corresponding to driving the system with a laser. Lower part: upgrading the classical sources of the upper panel with SPS. (c) is the counterpart of (a), to be referred to as the "incoherent SPS." The coherent case yields two very different types of quantum light at low and high pumping: (d) the coherent SPS and (e) the Mollow Photon Source (Mollow PS) which can emit more than one photon at a time. Other types of quantum sources and other types of targets constitute the topic of our future work.

it is a more general case that includes classical excitation as a particular case), but also comes with many more and higher degrees of freedom. This did not lead so far, to the best of our knowledge, to a classification. Tentatively, this could be provided in a first approximation by $g^{(2)}$ (antibunching, uncorrelated, bunching, superbunching). Since squeezed states have the correlations of coherent states, however, and they are precisely the type of input that motivated a new formalism, it is clear that this is still far from appropriate. We decided to approach this general problem by considering the following:

(i) the same optical target (here a harmonic oscillator, in Paper II [53] a two-level system),

(ii) the same type of quantum source (here and in Paper II [53], a SPS, in future work, an N-photon emitter),

(iii) both coherent and incoherent regimes,

(iv) both low and high pumping regimes.

The SPS is a good starting point because it is the paradigm of quantum light and is the most common light of this type in the laboratory. Exciting the harmonic oscillator makes the problem both simple and fundamental, so this is also a good starting point. While we have considerably restrained the possibilities, there still remains much to be explored and the following will only address the main results. The two types of excitations [aforementioned (a) and (b)] yield quite different types of SPS, that are introduced in the beginning of their respective sections, and are summarized in Table I. Note that in the table, the last row also includes the second one (which is the limit of small pumping). They are, however, so distinct qualitatively that it is helpful to think of them as separate sources. As we will show, the second row (small coherent pumping) leads to the best antibunching in the target.

IV. CHARTING THE HILBERT SPACE

Prior to considering which quantum states of the harmonic oscillator one can access by exciting it with various types of SPS, one needs a road map to characterize all of the states at a glance. The Hilbert space is a big place. Human's capacity of abstraction gives a deceivingly simple picture of it. The canonical basis of Fock states $|n\rangle$ with $n \in \mathbb{N}$ provides a comprehensive and concise map of the states in the harmonic oscillator's Hilbert space $\mathcal{H}_\infty$:

$$|\psi\rangle = \sum_{n=0}^{\infty} \alpha_n |n\rangle, \tag{6}$$

with $\alpha_n \in \mathbb{C}$ such that $\sum_{n=0}^{\infty} |\alpha_n|^2 = 1$. This is as precise as it is misleading since this fails to provide a qualitative

map of the possible states. Instead, one uses families of particular cases. Beyond Fock states per se, one makes a great use of the coherent states of classical physics, for which $\alpha_n = \alpha^n \exp(-|\alpha|^2)/\sqrt{n!}$ for some complex number α that defines the amplitude and phase of a classical field. The next family of important states requires the concept of mixity that involves statistical averages and upgrades the wave function to a density matrix:

$$\rho = \sum_{n,m=0}^{\infty} \beta_{nm} |n\rangle \langle m|. \tag{7}$$

This allows the introduction of thermal states, for which $\beta_{nm} = (1 - \theta)\theta^n \delta_{nm}$ for some reduced temperature $\theta \in [0,1]$. These two families can be united into a larger class of "cothermal"[54] states that interpolate between the two and describe, e.g., single-mode Bose condensates not too far from threshold. From there on, one essentially deals with quantum states of light with popular examples such as squeezed states [55], cat states [56], etc., and other less popular such as binomial states [57] or displaced Fock states [58]. Such a zoology of states is familiar to every quantum physicist, but it fails to provide the sought mapping of the Hilbert space. In particular, it is restricted to known (and popular) cases and leaves most of Eqs. (6) and (7) uncharted.

We introduce a map of the Hilbert space based on important observables for the quantum state, namely, the nth-order correlation functions:

$$g^{(n)} = \frac{\langle a^{\dagger n} a^n \rangle}{\langle a^\dagger a \rangle^n}. \tag{8}$$

Since we consider only the quantum states and not their dynamics, normalization makes $g^{(1)}$ trivially unity. We therefore use instead the normalization itself, which is an important observable, the population of the state (average number of excitations), for which we introduce the notation:

$$n_a \equiv \langle a^\dagger a \rangle. \tag{9}$$

Note that only the diagonal elements $p(m) = |\alpha_m|^2$ are needed so there is no distinction between pure and mixed states in this discussion. The nth-order correlator reads:

$$g^{(n)} = \frac{\sum_{m=0}^{\infty} m! p(m)/(m-n)!}{\left[\sum_{m=0}^{\infty} m p(m) \right]^n}. \tag{10}$$

A convenient mapping of the Hilbert space is to chart it with its population and statistical property "rulers", that is, tag the possible quantum states through their joint $g^{(2)}$ and n_a. The value of $g^{(2)}$ allows to tell apart classical from quantum

TABLE I. Characteristics of a SPS driven incoherently or coherently. In the latter case, for clarity, we also consider separately the low-driving intensity (middle row) from the general case (bottom row) that covers all pumpings, to highlight the strong qualitative features of the Mollow regime.

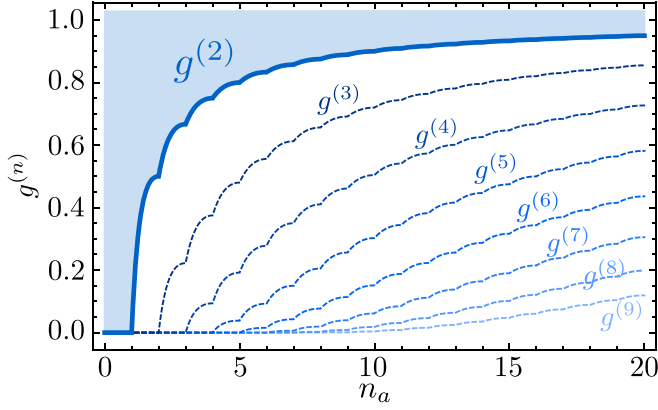| Source	Pumping	Population n_σ	$g_\sigma^{(2)}(\tau)$	Line shape	Linewidth
Incoherent SPS	P_σ	$P_\sigma/(\gamma_\sigma + P_\sigma)$	$1 - \exp[-(\gamma_\sigma + P_\sigma)\tau]$	Lorentzian	$\gamma_\sigma + P_\sigma$
Coherent SPS	Small Ω_σ	$4\Omega_\sigma^2/\gamma_\sigma^2$	$[1 - \exp(-\gamma_\sigma \tau/2)]^2$	Lorentzian	γ_σ
Coherent SPS	Large Ω_σ	$4\Omega_\sigma^2/(\gamma_\sigma^2 + 8\Omega_\sigma^2)$	$1 - e^{-\frac{3\gamma_\sigma \tau}{4}} \cos(2\Omega_\sigma \tau)$	Triplet	$\begin{cases} \gamma_\sigma \text{(central)} \\ 3\gamma_\sigma/2 \text{(satellites)} \end{cases}$

FIG. 2. Charting the Hilbert space. The shaded area shows the region where a physical quantum state exists with the corresponding joint population and antibunching. It is delimited by the boundary (11) of "Fock duos," defined by Eq. (12). Higher-order correlators (thin dashed) set other boundaries, also delimited by Fock duos.

states depending on whether $g^{(2)}$ is larger (bunching) or smaller (antibunching) than unity. This is meant in the sense of whether a classical, possibly stochastic, description is possible, or whether some "quantum" features such as violation of Cauchy-Schwarz inequalities or negative probabilities in the phase space are manifest. The population gives another meaning to quantumness, in the sense of few-particle effects versus macroscopic occupation. It is therefore particularly interesting to contrast these two attributes and consider, e.g., highly occupied genuinely quantum states. There is a physical limit to such states and for populations $n_a > 1$, some values of antibunching are out of reach. This is expected on physical grounds from familiar features of the Fock states popularly known as being the "most quantum" states, with their $g^{(2)}$ tending to one as the number of excitations increases. Also, macroscopic quantum states, such as a BEC, are essentially coherent states in most formulations. Here, we make this notion precise by providing the complete picture, in Fig. 2, along with the closed-form expression for the boundary that separates accessible combinations from impossible ones (this is proved in the Appendix A):

$$g^{(2)} = \frac{\lfloor n_a \rfloor (2n_a - \lfloor n_a \rfloor - 1)}{n_a^2}. \tag{11}$$

This boundary is provided by superpositions of contiguous Fock states, i.e., of the type:

$$\sqrt{p(n)}|n\rangle + \sqrt{1-p(n)}e^{i\theta}|n+1\rangle, \tag{12}$$

for $n \in \mathbb{N}$, $p(n) \in [0,1]$, and $\theta \in [0,2\pi[$ an (irrelevant) phase. (As already commented, this includes also mixed states of the type $p(n)|n\rangle\langle n| + [1-p(n)]|n+1\rangle\langle n+1|$ and all others with the same diagonal but different off-diagonal elements. We will not make this distinction anymore in the following.) We call these states, Eq. (12), "*Fock duos*." They set the continuous lower limit of the space of available quantum states in our charted Hilbert space. Their antibunching (11) is a generalization to noninteger n_a of the formula $g^{(2)} = 1 - 1/n_a$ for the Fock state $|n_a\rangle$ to which it reduces for $n_a \in \mathbb{N}$. It shows that the popular "single-particle criterion" that

asserts that $g^{(2)} < 0.5$ ensures a one-particle state [4,59–62] is wrong, as demonstrated, e.g., for the case $n_a = 1.5$ for which $g^{(2)} = 4/9 \approx 0.44$. The generalization to higher orders is straightforward. Namely, the nth-order correlation frontier for real n_a is given by:

$$g^{(n)} = \frac{\lfloor n_a \rfloor!}{(\lfloor n_a \rfloor - n)!n_a^n}\left[1 + \frac{n(n_a - \lfloor n_a \rfloor)}{\lfloor n_a \rfloor + 1 - n}\right], \tag{13}$$

that generalizes the Fock state formula $g^{(n)} = (1/n_a^n)m!/(m - n_a)!$ valid for integer n_a where it agrees with Eq. (13). Interestingly, the lower limit is also set, for all n, by Fock duos (not "n-plets").

One can also consider other charts of the Hilbert space, such as $(g^{(2)}, g^{(3)})$, contrasting two- and three-particle correlations together. This time there are no boundaries in this space (one can find a state with any joint values of $g^{(2)}$ and $g^{(3)}$). The proof of this statement is given in Ref. [63]. Since the excitation of a harmonic oscillator by the SPS leads to strong correlations between various $g^{(n)}$, we will focus on the $(n_a, g^{(2)})$ space.

V. EXCITING WITH AN INCOHERENT SPS

Now that we can conveniently characterize the states of the harmonic oscillator that one can excite, we come back to the dynamical problem of the quantum driving of a harmonic oscillator and how close one can get to the limit set by Eq. (11). We first consider the case of excitation with an incoherent SPS, i.e., where the two-level system (2LS) that acts as the source, is itself driven incoherently, as sketched in Fig. 1(c). Namely, there is a constant rate P_σ at which the 2LS is put in its excited state, and is otherwise left to decay. The system is thus described by the master equations (2) and (3), with $c_1 = \sigma$ the 2LS and $c_2 = a$ the harmonic oscillator operators, respectively. The 2LS pumping is described by a Lindblad term $(P_\sigma/2)\mathcal{L}_{\sigma^\dagger}\rho$. Thanks to the absence of feedback, the dynamics is ruled by closed equations which allow us to obtain exact solutions for the observables of interest. Namely, we find that the target (e.g., a cavity mode)'s population n_a and statistics $g^{(2)}$ are given by (cf. Table I for the source):

$$n_a = \frac{4P_\sigma\gamma_\sigma}{(\gamma_\sigma + P_\sigma)(\gamma_\sigma + P_\sigma + \gamma_a)}, \tag{14a}$$

$$g^{(2)} = \frac{2(\gamma_\sigma + P_\sigma)}{\gamma_\sigma + P_\sigma + 3\gamma_a}. \tag{14b}$$

Only two parameters are required to describe fully the system: (i) the ratio between the decay rate of the cavity and the emission rate of the 2LS, γ_a/γ_σ, and (ii) the intensity (or pumping rate) of the 2LS, P_σ, also normalized to γ_σ to keep the parameters dimensionless. Eliminating P_σ from Eqs. (14), this gives the equation for the trajectory in the $(n_a, g^{(2)})$ space as function of the parameter γ_a/γ_σ:

$$n_a = \frac{2}{3}\frac{(2 - g^{(2)})[3g^{(2)}(\gamma_a/\gamma_\sigma) - (2 - g^{(2)})]}{g^{(2)}(1 + g^{(2)})(\gamma_a/\gamma_\sigma)}. \tag{15}$$

These trajectories in the Hilbert space are plotted in Fig. 3. The curves start from the point:

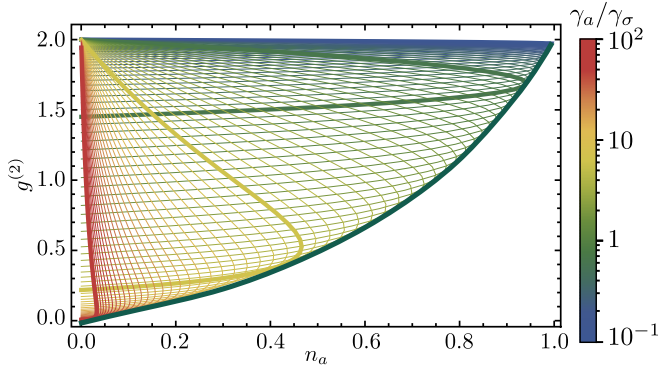$$\left(n_a = 0, \; g^{(2)} = \frac{2}{1 + 3\gamma_a/\gamma_\sigma}\right), \tag{16}$$

FIG. 3. Trajectories in the Hilbert space charted by n_a and $g^{(2)}$ for the states excited by an incoherent SPS, for various values of γ_a/γ_σ. The implicit parameter is pumping. Highlighted are the cases $\gamma_a/\gamma_\sigma = 10^{-1}$ (blue), 1 (green), 10 (yellow), and 10^2 (red). The dark green thick envelope shows the closest one can get in this configuration to the ideal antibunching, which is zero. All the states, and only these states, above this line and below $g^{(2)} = 2$, are accessible with an incoherent SPS.

at vanishing pumping, reach a turning point with coordinates:

$$\left(n_a = \frac{4[2 + (\gamma_a/\gamma_\sigma) - 2\sqrt{1 + (\gamma_a/\gamma_\sigma)}]}{(\gamma_a/\gamma_\sigma)^2}, \right.$$

$$\left. g^{(2)} = \frac{2}{3\sqrt{1 + \gamma_a/\gamma_\sigma} - 2} \right), \qquad (17)$$

when $P_\sigma = \sqrt{\gamma_\sigma(\gamma_a + \gamma_\sigma)}$ and converge at $(n_a = 0, g^{(2)} = 2)$ at large pumpings, where the source gets quenched. For each

value of γ_a/γ_σ, there are two values of pumping that result in the same population but two values of $g^{(2)}$. The curve of Eq. (15) is fairly constant until the turning point and, from Eq. (16), allows a genuine quantum state (i.e., featuring antibunching) as long as $\gamma_a/\gamma_\sigma > 3$, which means that, with a SPS, one can imprint antibunching in a system that has a substantially longer lifetime. The optimum antibunching and population for a given γ_a/γ_σ is achieved when $P_a \approx \gamma_\sigma$, that is, slightly before the turning point. The envelope of all the curves in Fig. 3 is the closest one can get to the Fock-duos limit, and is given by $g^{(2)} = 2n_a/(3 - 2n_a)$. This is the thick dark green line in Fig. 3.

The above solution gives an already substantial description of the response of a harmonic oscillator to an incoherent SPS. We can complement it with alternative descriptions that approach the solution from different viewpoints and manifest the advantage of cascaded coupling over other types of excitation. A natural comparison is with the standard Hamiltonian coupling, that is the usual way to couple different systems. For instance, it is convenient to lay out the observables as function of the parameters in 2D density plots, as shown in the upper row of Fig. 4. Figures 4(a)–4(c) show the photon statistics (color code) and the population of the cavity (isolines) using the (a) cascaded coupling and (b), (c) the Hamiltonian coupling. For the latter case, we consider two configurations: (b) when the 2LS has the same decay term as when acting as a source in the cascaded scheme, and (c) when the 2LS has no decay term, so that all its excitation is directed towards the cavity, corresponding to the ideal excitation of the cascaded scheme. Interestingly, (a) and (b) types of excitation present a qualitatively similar photon statistics layout, but the topography of the resulting population yields largely
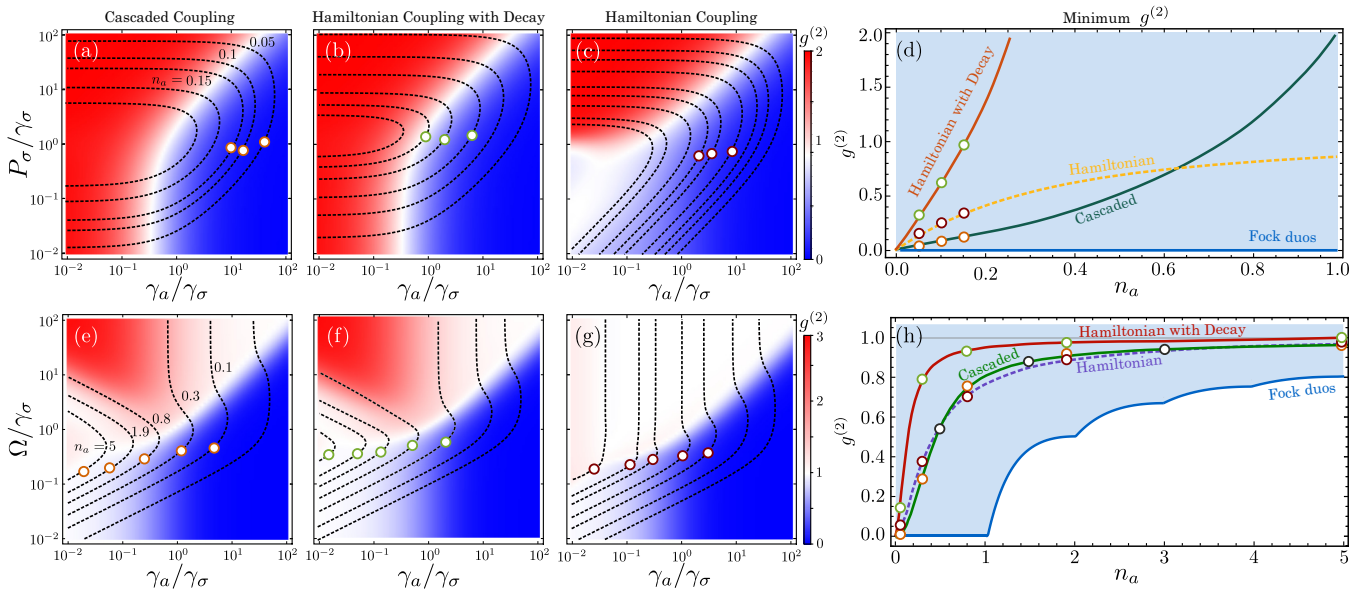

FIG. 4. Upper row: populations (isolines) and $g^{(2)}$ (color) of the target excited by an incoherent SPS, through (a) the cascaded coupling or (b), (c) the Hamiltonian coupling with (b) and without (c) decay of the 2LS. (d) Minimum $g^{(2)}$ that can be reached at a given population for all these cases. The color circles mark the parameters P_σ/γ_σ and γ_a/γ_σ at which the population isoline meets the minimum $g^{(2)}$. Lower row: same but for a coherent SPS, with (e) the cascaded coupling and (f), (g) the Hamiltonian coupling with (f) and without (g) decay of the 2LS. (h) Minimum $g^{(2)}$ that can be reached at a given population for all these cases. The color circles mark the parameters $\Omega_\sigma/\gamma_\sigma$ and γ_a/γ_σ at which the population isoline meets the minimum $g^{(2)}$.

differing states, as evident once reported in the $(n_a, g^{(2)})$ space, Fig. 4(d). The color circles along the isolines mark the points with strongest antibunching (i.e., smallest $g^{(2)}$) for a given population. It is seen that for a given signal, the antibunching is significantly larger with the cascaded coupling. In both cases, the antibunching is marred before the cavity population reaches one photon on average. At larger populations, the photon statistics of the cavity become bunched, i.e., $g^{(2)} = 2$. On can contemplate other configurations but they result in worse results: detuning the cavity from the 2LS leaves the photon statistics unchanged, but reduces the population of the cavity, so the antibunching is lost at even smaller cavity populations. Dephasing the 2LS increases the broadening of the emission peak, but also drives the cavity towards a coherent state faster. Hamiltonian coupling with no decay of the 2LS, case (c), differs qualitatively from the former cases and provides a substantially better antibunching than Hamiltonian coupling with decay of the 2LS. It even becomes better than the cascaded coupling when $n_a \gtrsim \frac{2}{3}$. This situation can be much improved with the coherent SPS.

VI. EXCITING WITH A COHERENT SPS

We now consider excitation by a coherent SPS, i.e., when the 2LS that acts as the source is driven coherently by an external laser, as sketched in Fig. 1(d). This driving is described by the Hamiltonian:

$$H_\sigma = \omega_\sigma \sigma^\dagger \sigma + \Omega_\sigma \sqrt{\epsilon_1}(\sigma^\dagger e^{-i\omega_L t} + \sigma e^{i\omega_L t}), \qquad (18)$$

where ω_σ is the energy of the 2LS, and ω_L and $\Omega_\sigma = \sqrt{\gamma_\sigma}\mathcal{E}$ are the frequency and intensity of the driving laser (which drives a 2LS of decay rate γ_σ with a coherent field of intensity $\mathcal{E}$), respectively. The coefficient $\sqrt{\varepsilon_1}$ is put here, in agreement with Eq. (5), so that the cavity is driven only by the emission of the 2LS and not by the external laser, which would spoil the antibunching. The system is otherwise still described by the master equations (2) and (5), with $c_1 = \sigma$ the 2LS (source) and $c_2 = a$ the harmonic oscillator (target), and reducing the coupling strength by a factor $\sqrt{1 - \epsilon_1}$, i.e., the coupling is given by $\sqrt{(1 - \epsilon_1)\gamma_a \gamma_\sigma}$. Here again, one can obtain the cavity observables in closed form, although it takes slightly more cumbersome expressions. At resonance (out-of-resonance cases can also be obtained but get even more bulky),

$$n_a = \frac{16(1 - \epsilon_1)\gamma_{\tilde{0}\tilde{1}}\Omega_0^2\left(\gamma_{\tilde{1}\tilde{1}}^2\gamma_{\tilde{1}\tilde{2}} + 8\gamma_{\tilde{1}\tilde{0}}\Omega_0^2\right)}{\gamma_{\tilde{1}\tilde{0}}\gamma_{\tilde{1}\tilde{1}}\left(\gamma_{0\tilde{1}}^2 + 8\Omega_0^2\right)\left(\gamma_{\tilde{1}\tilde{1}}\gamma_{\tilde{1}\tilde{2}} + 16\Omega_0^2\right)}, \qquad (19a)$$

$$g^{(2)} = \frac{\gamma_{\tilde{1}\tilde{1}}\left(\gamma_{0\tilde{1}}^2 + 8\Omega_0^2\right)\left(\gamma_{\tilde{1}\tilde{1}}\gamma_{\tilde{1}\tilde{2}} + 16\Omega_0^2\right)\left[\gamma_{\tilde{1}\tilde{1}}\gamma_{\tilde{2}\tilde{1}}^2\gamma_{\tilde{3}\tilde{1}}^2\gamma_{\tilde{1}\tilde{2}}\gamma_{\tilde{3}\tilde{2}} + 8\gamma_{\tilde{1}\tilde{0}}\gamma_{\tilde{3}\tilde{1}}(17\gamma_{\tilde{1}\tilde{0}}^3 + 29\gamma_{\tilde{1}\tilde{0}}^2\gamma_{0\tilde{1}} + 18\gamma_{\tilde{1}\tilde{0}}\gamma_{0\tilde{1}}^2 + 4\gamma_{0\tilde{1}}^3)\Omega_0^2 + 192\gamma_{\tilde{1}\tilde{0}}^2\gamma_{\tilde{2}\tilde{1}}\Omega_0^4\right]}{\gamma_{\tilde{2}\tilde{1}}\gamma_{\tilde{3}\tilde{1}}\left(\gamma_{\tilde{1}\tilde{1}}\gamma_{\tilde{2}\tilde{1}} + 8\Omega_0^2\right)\left(\gamma_{\tilde{3}\tilde{1}}\gamma_{\tilde{3}\tilde{2}} + 16\Omega_0^2\right)\left(\gamma_{\tilde{1}\tilde{1}}^2\gamma_{\tilde{1}\tilde{2}} + 8\gamma_{\tilde{1}\tilde{0}}\Omega_0^2\right)^2}, \qquad (19b)$$

where we have introduced the notation $\gamma_{\tilde{i}\tilde{j}} = i\gamma_a + j\gamma_\sigma$ (e.g., $\gamma_{\tilde{3}\tilde{1}} = 3\gamma_a + \gamma_\sigma$), and we have set $\Omega_0 = \sqrt{\epsilon_1}\Omega$. Eliminating Ω^2 from Eqs. (19) yields, for a given γ_a/γ_σ, solutions of the type $g^{(2)} = (P[3] \pm \sqrt{P[6]})/(P[2]n_a^2)$ where $P[n]$ is an nth-order polynomial of the variable n_a. The $\pm$ terms provide the two branches of the curve as seen in Fig. 5(a). The lower branch corresponds to low pumping, where the photoluminescence (PL) of the source is still a single line as shown in the bottom inset, while the upper branch corresponds to high pumping where the PL has split into a Mollow triplet, shown in the upper inset. Each curve starts from the point:

$$\left(n_a = 0, \; g^{(2)} = \frac{1}{(1 + \gamma_a/\gamma_\sigma)^2}\right), \qquad (20)$$

showing that coherent SPS provide a much stronger antibunching than their incoherent counterpart, Eq. (16), already at vanishing pumping. At high pumping, in contrast to the incoherent case that vanishes the population of its target, the coherent SPS quenches it to a nonzero value and featuring bunching:

$$\left(n_a = \frac{1 - \epsilon_1}{1 + \gamma_a/\gamma_\sigma}, \; g^{(2)} = 3\frac{1 + \gamma_a/\gamma_\sigma}{1 + 3\gamma_a/\gamma_\sigma}\right). \qquad (21)$$

Eliminating γ_a/γ_σ here leads to the curve $g^{(2)} = 3(1 - \epsilon_1)/[3(1 - \epsilon_1) - 2n_a]$, which for $\epsilon_1 = \frac{1}{2}$ simplifies to $g^{(2)} = 3/(3 - 4n_a)$ as shown in thick black in Fig. 5(a). The expression for the lower envelope of maximum antibunching,

in blue, is too complicated to be derived fully in closed form but we can find simple asymptotic expressions by series expansion of Eqs. (19), namely, $g^{(2)} \approx 5n_a^2$ when $n_a \ll 1$ and $g^{(2)} \approx 1 - 1/[3(n_a + 5)]$ when $n_a \gg 1$. The states thus get close to the ideal Fock limit for large populations, approaching unity as $1/(3n_a)$ rather than $1/n_a$. There is no limit in the population that can be excited in the target by the coherent SPS, in stark contrast to the incoherent SPS that is bounded by unity. Although the accessible states in the $(n_a, g^{(2)})$ space remain quite some distance away from the theoretical limit, the coherent SPS provides a much better antibunching than its incoherent counterpart, as can be seen by comparing Figs. 3 and 5. Namely, it is still antibunched when population is unity (with a maximum antibunching slightly over $\frac{1}{2}$) and we have already commented how it allows for arbitrary large populations, that still feature antibunching. This is achieved by exciting at resonance targets of very long lifetimes as compared to the source.

This describes the resonant situation. Since the coherent SPS has a rich spectral structure, it opens new configurations of excitation in the Mollow triplet regime beyond the central peak, such as exciting with a satellite peak [as shown in Fig. 5(c)] or with the leapfrog window [Fig. 5(b)]. In these cases, we show the results in log-log plots as only small populations are within reach (unlike the case of resonance) and, in the case of leapfrog excitation, also a huge bunching can be imparted to the target. The envelope of optimum antibunching as obtained in resonance is reported in these panels (also
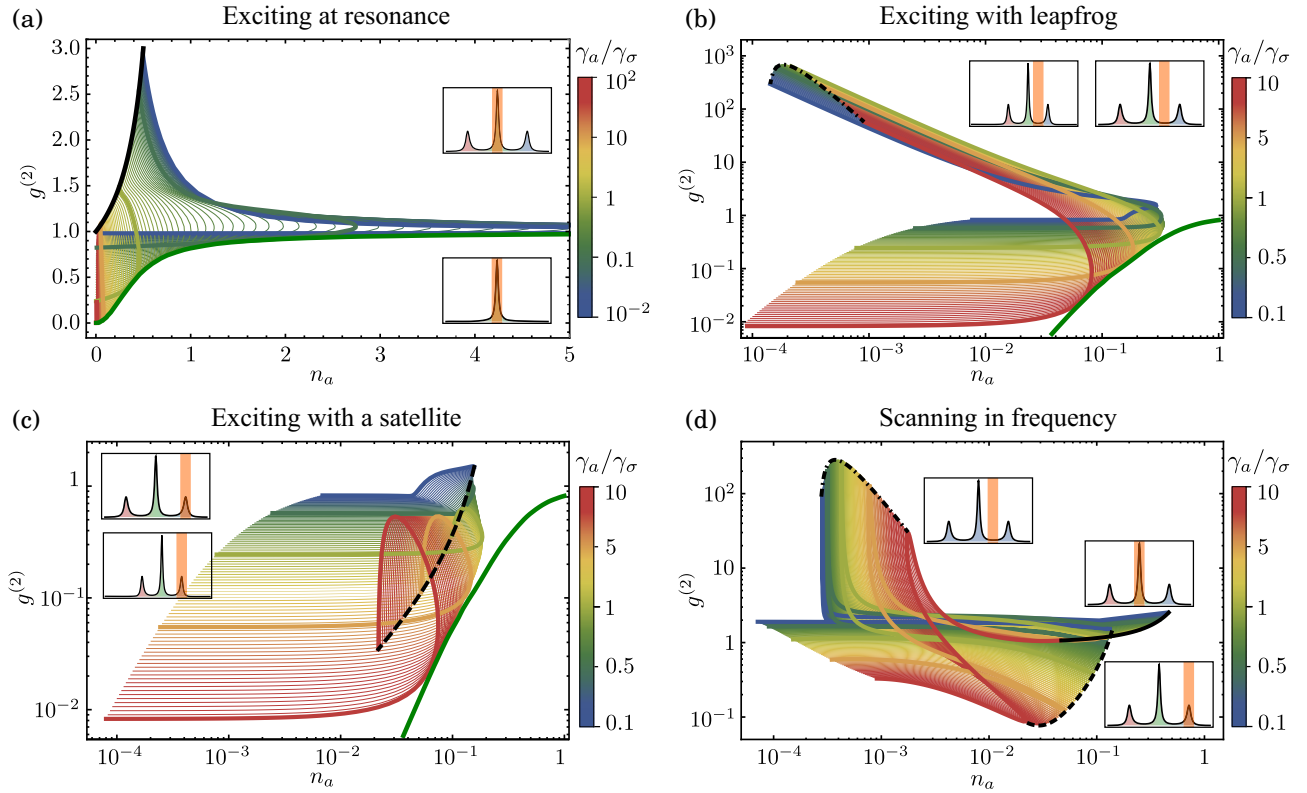
FIG. 5. Same as Fig. 3 but for the excitation from a coherent SPS. In (a-c) the implicit parameter is pumping and the green line shows the closest one can get from the Fock-duos limit from the case at resonance. In (d) the implicit parameter is the detuning between the source and its target. (a) Excitation at resonance. The optimum antibunching is the envelope in this configuration of the family of curves varying with γ_a/γ_σ. Highlighted are the cases $\gamma_a/\gamma_\sigma = 10^{-2}$ (blue), 10^{-1} (green), 1 (chartreuse), 10 (yellow), and 10^2 (red). (b)–(d) Excitation in other configurations, namely (b) with the leapfrog processes, (c) with the satellite, and (d) as a function of frequency. Highlighted are the cases $\gamma_a/\gamma_\sigma = 10^{-1}$ (blue), 0.5 (chartreuse), 1 (green), 5 (orange), and 10 (red). The dashed-dotted line in panel (b) and the dashed line in panel (c) show the limit of large intensities and are merely a visual aid rather than a physical boundary. They are also shown in panel (d), along with the black solid line for the envelope of the curves at $\omega_a = \omega_\sigma$.

in green) for comparison, showing that these alternative schemes do not enhance antibunching. The excitation with leapfrog processes allows to access new regions of the Hilbert space related to superbunching, so it is a configuration that presents its own interest. This is achieved at the price of small populations. Excitation with a satellite peak also conquers new territories in the $(n_a, g^{(2)})$ space not accessible through either the central peak or leapfrog emission in a small region ($n_a \approx 0.6$, $g^{(2)} \lesssim 2$). Figure 5(d) shows the trajectories when varying the frequency of emission, where the cases just discussed, resonance, leapfrog, and satellites, appear as boundaries of the complete picture, thus showing that these configurations already give access to all the accessible states.

We can also compare in the parameter space the coherent SPS with its Hamiltonian counterpart, as we did for the incoherent SPS. This is shown in the bottom row of Fig. 4, that is also usefully compared with the upper row (incoherent SPS excitation). For the coherent SPS as well, both cascaded and Hamiltonian coupling are qualitatively similar in their statistical layout when the 2LS has a decay term, but also differ from the topography of the associated intensities. This is, again, clear on the $(n_a, g^{(2)})$ space, with the maximum antibunching that can be obtained for a given cavity population with cascaded coupling (green line) and Hamiltonian coupling

(red line). The Hamiltonian coupling with no decay of the 2LS also results in qualitative differences and an enhanced antibunching. However, in this case, the Hamiltonian coupling never comes to surpass the cascaded scheme. Instead, in all the range of population, the antibunching obtained through the cascaded coupling is larger than the one obtained with any type of normal (Hamiltonian) coupling, for a given population. When the cavity is detuned from the 2LS, the antibunching is lost before the cavity's population reaches one photon. Also, when the cavity is in resonance with the leapfrog process emission, the photon statistics of the cavity is superbunched but its population remains well below unity. Including a dephasing rate to the dynamics of the 2LS increases the broadening of each emission line in the triplet, and even a small dephasing rate spoils the antibunching. Thus, the best antibunching with a coherent SPS is obtained exciting the cavity at low pumping and in resonance with the 2LS, using the cascaded coupling.

One of the departing features of the coherent SPS excitation is that it allows to populate its target with more than one excitation on average, therefore triggering Bose stimulation effects. There is a phase locking (of 0, as determined by the Hamiltonian) of the incident photons from the quantum source that accumulates while still exhibiting some features of Fock states, in particular being antibunched. A complete picture of
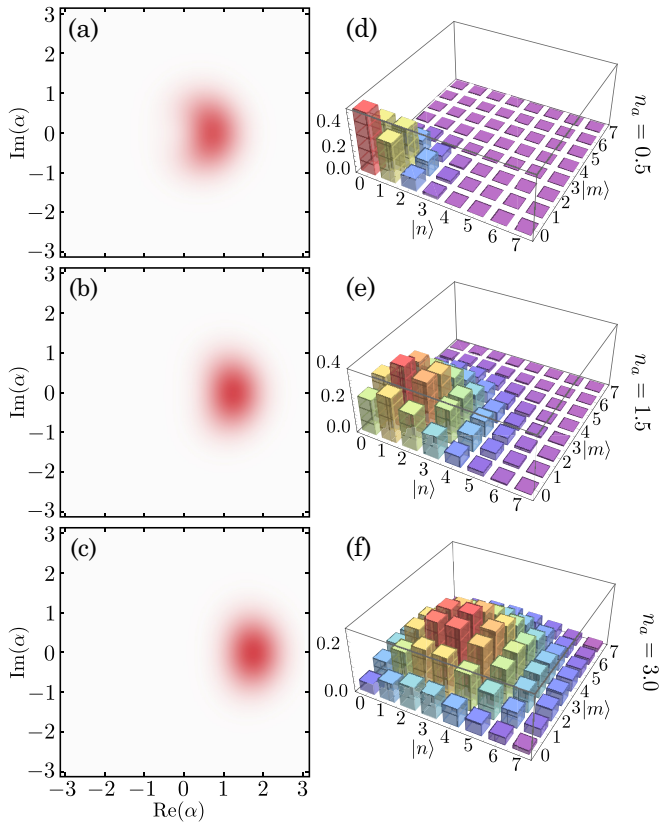
FIG. 6. Wigner function (a)–(c) and density matrix (d)–(f) for the states marked by black circles along the green line in Fig. 4(h). These states have populations $n_a = 1$, 1.5, and 3 from top to bottom and all feature antibunching.
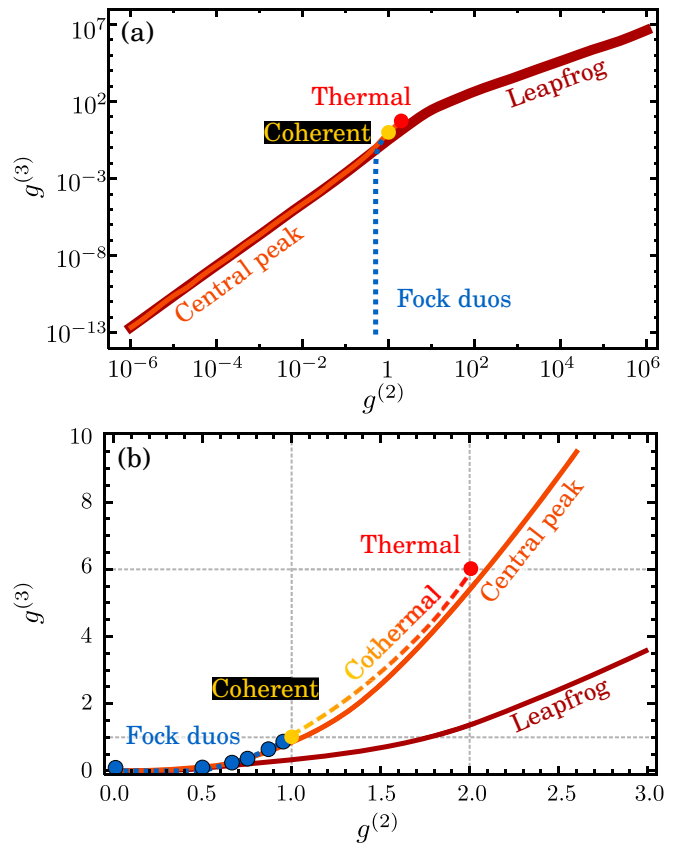

FIG. 7. States accessible in the $(g^{(2)}, g^{(3)})$ space by coherent SPS excitation, at resonance with the central peak (orange line) or with the leapfrog emission (red line). The dashed blue line corresponds to the "Fock duos" [Eq. (A1)]. The same result is shown in both (a) log-log and (b) linear scales.

the resulting quantum states, beyond the diagonal elements only, is given Fig. 6 for the states marked with black circles in Fig. 4(f), both through the Wigner representation [Fig. 6(a)–6(c)] and through their matrix representation [Figs. 6(d)–6(f)]. It is positive everywhere, although the state is still antibunched. Also, one can see that the phase uncertainty decreases as the population increases, in agreement with the "classical limit." Moreover, the matrix elements in these cases also satisfy the relation $\rho_{22} > \max(\rho_{11}/2, \rho_{33})$, which means that fluctuations are smaller than could be expected from rate-equation arguments since two excitations are twice as much likely to decay than one excitation, making the probability to find one excitation only in principle at least twice as large than double occupation [26].

We conclude this section on driving a harmonic oscillator with the coherent SPS by considering states in the $(g^{(2)}, g^{(3)})$ space. This is shown in Fig. 7 for the most notable configurations of exciting with the central peak of the Mollow triplet or the leapfrog region between the central peak and a satellite. All points are physical on this map, including cases with $g^{(2)} \ll 1$ and $g^{(3)} \gg 1$ (and vice versa), although the accessible regions are strongly confined along curves that we can fit in monomial form, leading in good approximation to $g^{(3)} \approx 0.2[g^{(2)}]^2$ at low pumping (in the antibunching corner) and $g^{(3)} \approx 4.5g^{(2)}$ at large pumpings (in the superbunching corner). We indicate positions of popular quantum states such as Fock states, coherent states, thermal states, and their

combinations. Driving with a SPS spans over great distances in this space, especially when exciting with leapfrog processes, as seen in Fig. 7(a) of the figure. This shows, again, how the central peak remains confined essentially to the antibunched corner of the map (excursions to bunching cases are up to $g^{(2)} = 3$). Figure 7(b) is a zoom around small values in linear scale. The leapfrog processes, on the contrary, allow one to reach large joint values of $g^{(2)}$ and $g^{(3)}$. Interestingly, while the points accessible in the $(n_a, g^{(2)})$ space extend over two-dimensional (2D) areas, in the $(g^{(2)}, g^{(3)})$ space they are confined to one-dimensional (1D) curves, showing how these correlators are strongly interdependent, and thus making the $(n_a, g^{(2)})$ representation more prominent.

VII. VARIATIONS IN THE TYPE OF COUPLING

The comparison between both rows of Fig. 4 shows that the coherent SPS is a much better quantum drive to generate bright antibunching than the incoherent one, even in the region where $n_a < 1$. The coherent SPS exciting the cavity still remains some distance away from the Fock-duos boundary, but it gets closer than with the Hamiltonian coupling. We complete our juxtaposition between the two types of coupling, cascaded and Hamiltonian, by comparing with other variations in the way the source couples to its target.
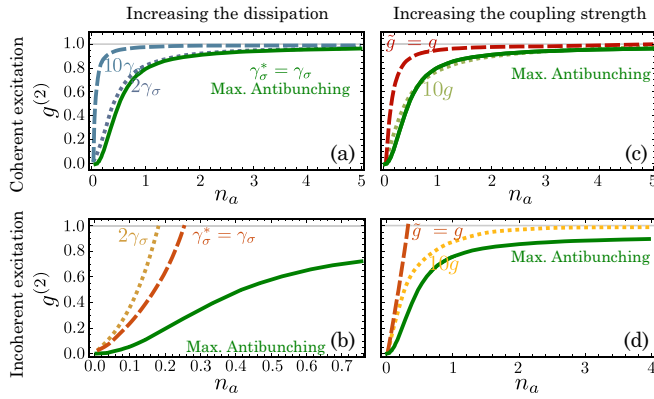
FIG. 8. Variations in the model. (a), (b) Adding a dissipative channel to the source in the cascaded coupling spoils the antibunching. (c), (d) Increasing the coupling strength g in the Hamiltonian coupling (with decay in the source) enhances the antibunching until it reaches the one obtained for the Hamiltonian coupling without decay of the source (when $\tilde{g} \approx 10g$). However, the enhancement is never enough to top the antibunching obtained using the coherently driven 2LS and the cascaded coupling.

First, we consider another source of decay for the source in the cascaded coupling scheme, i.e., with an extra term $(\gamma_\sigma^*/2)\mathcal{L}_\sigma \rho$ in the master equation, leaving the coupling strength constant and equal to $\sqrt{\gamma_a \gamma_\sigma}/2$. This describes the situation where not all the light that is lost from the source is redirected to the target. Figures 8(a) and 8(b) show how this other source of decay spoils the antibunching and drives the cavity faster toward a coherent state (for the coherent SPS) or to a thermal state (for the incoherent SPS). At $\gamma_\sigma^* = 10\gamma_\sigma$, the antibunching is worse than that obtained using the Hamiltonian coupling (without any additional dissipative channel). This shows that it is better to minimize losses from the quantum emitter, but that unless these are drastic, the impact is moderately detrimental. Note that the cascaded coupling strength can only be smaller or at most equal to $\sqrt{\gamma_1 \gamma_2}$, unlike some statements in the literature [64] that refer to "arbitrary coupling strengths." This leads, otherwise, to unphysical states for the target. Second, in the Hamiltonian case, we increase the coupling strength and bring the system into the strong-coupling regime. This is one considerable degree of freedom of the Hamiltonian coupling that is lost when considering some external excitation since photons that drive the system from outside can couple to it in the first place because it is dissipative. In fact, the more efficient is the source-target coupling, the more dissipative the target has to be. But, a dissipative target cannot sustain quantum effects for long, as the states do indeed decay. Therefore, there is a compromise for the target's lifetime to allow simultaneously an efficient driving from the source while still allowing to store long enough the imprinted quantum attributes. In the Hamiltonian coupling, however, coupling and decay are independent and one can consider a pure Hamiltonian picture with no decay whatsoever. We will see in future work how one can remedy to this vicious circle to some extent by considering other types of quantum sources. For now, we show that, surprisingly, cascaded coupling indeed provides a better quantum driving than the Hamiltonian coupling brought in the strong-coupling

regime. This is because in the latter case, the reversible process from the "target" back to the "source" acts like an effective decay. This is shown in Figs. 8(c) and 8(d), where we compare again the maximum antibunching obtained in the configuration of Sec. VI (solid green lines) with a magnified Hamiltonian coupling $\tilde{g} = N\sqrt{\gamma_a \gamma_\sigma}/2$ for various N. For both the coherent and incoherent excitation cases, the antibunching is improved by raising the coupling strength. However, this improvement is still not large enough to overcome the cascaded coupling. As seen in the figure, even for large Hamiltonian coupling strengths, the antibunching obtained with the cascaded coupling (solid green line) is better at small populations where the antibunching is largest. Increasing even further the value of N does not improve the antibunching, but makes it occur at larger $(\Omega_\sigma, \gamma_a)$ values. At this limiting case, the antibunching obtained for the Hamiltonian coupling with the decay of the source coincides with the antibunching for the Hamiltonian without the decay of the source. Therefore, Fig. 8(c) shows the optimum antibunching that can be obtained using both the cascaded and Hamiltonian couplings.

Increasing the coupling has a much stronger effect in the case of incoherent excitation, as shown in Fig. 8(d). Even a small variation of the coupling strength, $N = 1.5$, changes significantly the curvature of the antibunching curve. Increasing the value of N makes the system enter the "one-atom laser" regime [65], and the state in the cavity becomes coherent. As for the coherent excitation, the best antibunching saturates with increasing coupling (converging at roughly $\tilde{g} = 10g$), with larger values of the coupling strength merely occurring at larger (P_σ, γ_a) values. Nevertheless, although raising the coupling strength improves the antibunching, and at large $\tilde{g}$ the $g^{(2)}$ of the cavity at large population goes to 1, the best antibunching is still obtained with the cascaded coupling in the coherent excitation regime [green line in Fig. 8(d)]. Overall, it is therefore established that optimum antibunching is obtained in the cascaded architecture. This could have important consequences in the design of future quantum-optical devices.

VIII. SUMMARY AND CONCLUSIONS

Our analysis of the excitation by a SPS of a quantum harmonic oscillator can be summarized by Fig. 9. Here, we show again the charting of the Hilbert space of the quantum harmonic oscillator that we have introduced, along with the various areas that can be accessed with a SPS. First, the region I of physical states, shown in light blue, delimited by Fock duos [Eq. (12)] according to Eq. (11). No state exists that can provide the corresponding joint population and antibunching in the white region. In contrast to popular belief, states do exist in the region above this boundary that satisfy $g^{(2)} < \frac{1}{2}$ and $n_a > 1$ which shows that on mathematical grounds, the criterion $g^{(2)} < \frac{1}{2}$ cannot be used to exclude states with more than one particle. In this region of physical states, the green area can be accessed in the steady state by exciting a cavity with a SPS, provided an adequate γ_a/γ_σ ratio and pumping. The largest span is realized by a coherent SPS (i.e., a 2LS itself driven by a laser) at resonance with its target. This gives access to the dark green region II. Not all the states from region I are accessible in this configuration, in particular
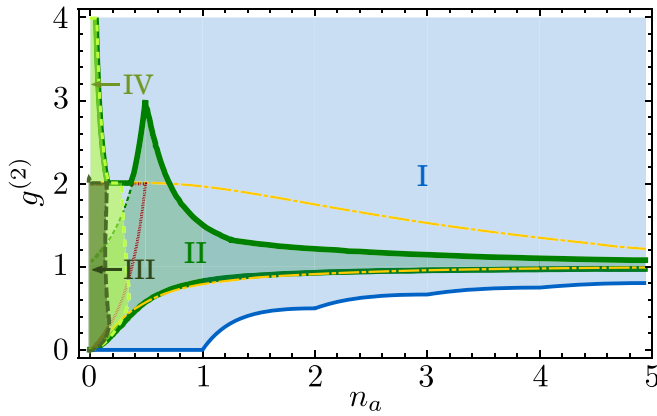
FIG. 9. Summary of our results: the Hilbert space of a harmonic oscillator charted by n_a (population) and $g^{(2)}$ (second-order correlation function) is accessible for any point in the blue region I (the white region is forbidden). Of this region, the wider span is achieved by exciting with a coherent SPS, covering the green region. This region breaks down into II, the region achieved at resonance between the source and the target, III, that achieved with the excitation from a satellite of the Mollow triplet and IV, that achieved with the leapfrog emission. The incoherent SPS covers a smaller region, delimited by the red dotted curve. The Hamiltonian coupling, between the two dotted-dashed yellow curves, also covers a large span of the Hilbert space and is neither included by, nor fully excluded of, the SPS area. In particular, the excitation by a SPS allows to provide a stronger antibunching at small populations where the antibunching is the largest, as compared to a Hamiltonian coupling, although it still remains some distance away from the theoretical limit.

the limit of Fock duos remains some distance away from the driven dissipative case. We will show in Paper II [53] of this work how one can get closer using other quantum sources. States of arbitrary populations can be reached with the coherent SPS (by using targets with long enough lifetimes) that still retain antibunching. One can also realize states of arbitrary high bunching, by using leapfrog emission of the SPS in the Mollow triplet regime. This is the region IV shown in light green in Fig. 9. Excitation with the satellite peaks covers the region III that gives access to a small patch not within reach of II and IV. Other frequencies do not lead to areas not already covered by these cases. The incoherent SPS does not extend this territory either, as it is contained in the area $2n_a/(3 - 2n_a) \leqslant g^{(2)} \leqslant 2$, shown in dotted red. Notably, the region accessible by the Hamiltonian regime does not include nor is included by that accessible with the cascaded coupling. They do share some common area. In fact, cascaded coupling reduces to Hamiltonian coupling whenever $g/\gamma_\sigma \ll \gamma_a/\gamma_\sigma$ which, for the cascaded coupling constraint of $g/\gamma_\sigma = \sqrt{\gamma_a/\gamma_\sigma}/2$, provides the criterion $\gamma_a/\gamma_\sigma \gg \frac{1}{4}$ for which the conventional formalism is enough to describe excitation with no feedback. This criterion allows, for instance, to develop the theory of frequency correlation [27] in a conventional setting without the explicit need of the cascaded formalism to prevent feedback, a point that has not always been fully appreciated [64]. In other cases, we have shown that cascaded coupling allows, surprisingly, to reach regions of the Hilbert space out of reach of a conventional Hamiltonian dynamics

and, in particular, to improve the possible antibunching for a given population.

IX. PERSPECTIVES

We have considered only one aspect of the general picture of quantum excitation of optical targets. Namely, various types of SPS exciting a harmonic oscillator. In the laboratory, this can take the form of exciting a passive cavity mode, or a noninteracting boson field. This is the configuration sketched in Fig. 10 I and that we addressed in this text, the opening one of a series that will carry on similar studies to other configurations of interest, as sketched in the rest of Fig. 10 and summarized here. In Paper II [53], we consider the problem of exciting a 2LS rather than the harmonic oscillator. In the future, we plan to increase one step more the level of complexity of the target by exciting polaritons, i.e., coupled light-matter systems. This focuses on different targets subjected to the (quantum) light of the same type of source. Also, we revisit all these targets together but now excited by an even "more quantum" source than the SPS, namely, N-photon emitters [66]. In addition, we will come back to all the combinations dealt with so far but turning to pulsed excitation rather than cw, addressing the problem of quantum state preparation. Even with this and future works taken together, we do not exhaust the topic and much remains to be studied even in the configurations put
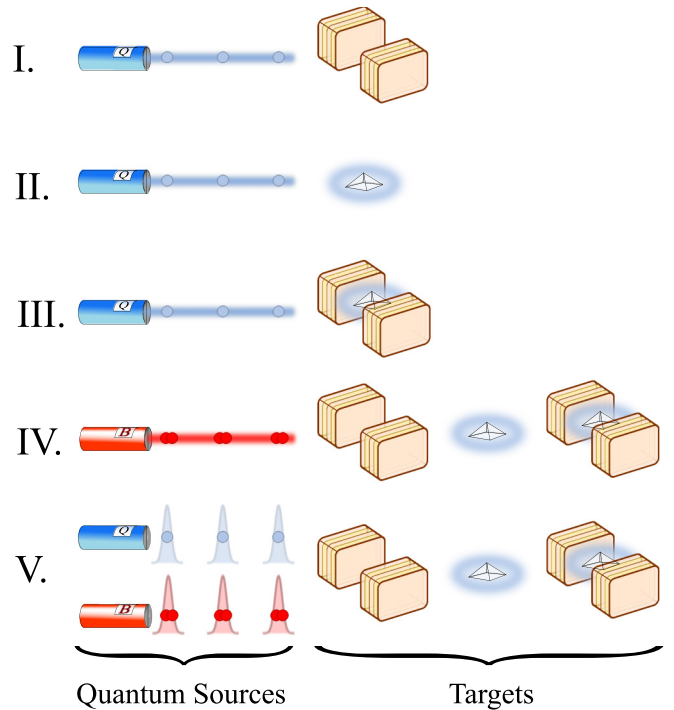

FIG. 10. Excitation with quantum light: the basic configurations we propose to study in this and future works. Paper I is the current work, exciting a harmonic oscillator (single-cavity mode) with a SPS. Paper II [53] addresses the excitation of a 2LS with a SPS. In the future we will study excited coupled light-matter systems, or polaritons, still with a SPS. Following the comprehensive treatments of these several targets under the cw excitation from a SPS, we then trade this simple quantum source for a N-photon emitter (bundler) and a pulsed quantum source, impinging on all the targets previously considered.

to scrutiny. For instance, we considered one particular type of SPS only, the simplest one as realized by a single emitter, while implementations from pairs of photons with one heralding the other [mainly through parametric down conversion (PDC) and four-wave mixing (FWM)] are extremely popular and with advantages of their own, such as determinism. It is clear that there is much engineering to be done with such sources as well, and certainly some improvements in their operating conditions to be gained from the cascaded architecture, e.g., helping to fix their principal drawback so far: the nonzero probability to emit more than a single photon. Also, this extended exploration of the general problem of quantum excitation will give us many occasions to revisit the same aspects from different angles. Already in Paper II [53], we will come back to the question of what regions of the Hilbert space are within reach. As another example, in future work, we will provide a clear physical picture of why the cascaded architecture allows such an enhancement as compared to the Hamiltonian coupling by considering the time-resolved excitation of the target by the spontaneous emission of an initial condition prepared in the source, which can be solved exactly. This brings much clarification into the nature of the target and the source and their interrelationship in a quantum context.

APPENDIX: PROOF THAT FOCK DUOS BOUND THE $(n_a, g^{(2)})$ SPACE

We prove mathematically that there are no states below the boundary set by Eq. (11) but at least one for every point above, thus showing that our charting of the Hilbert space in the $(n_a, g^{(2)})$ space as defined by this boundary is complete.

Proposition. For a given population $n_a \in \mathbb{R}$, the maximum antibunching is given by a superposition of at most two consecutive Fock states.

First, for any $n_a \in \mathbb{R}$, there exists a superposition of at most two consecutive Fock states that provides this population, namely,

$$\sqrt{\lfloor n_a \rfloor - n_a + 1}|\lfloor n_a \rfloor\rangle + \sqrt{n_a - \lfloor n_a \rfloor}|\lfloor n_a \rfloor + 1\rangle. \quad \text{(A1)}$$

We can write without loss of generality the generic state (6) as:

$$\sum_{k=-\lfloor n_a \rfloor}^{\infty} \sqrt{p(\lfloor n_a \rfloor + k)}|\lfloor n_a \rfloor + k\rangle, \quad \text{(A2)}$$

where we remind that $p(n) = |\alpha_n|^2$ and is such that $\sum_{n=0}^{\infty} p(n) = 1$. Restricting ourselves to states with the same population implies:

$$\sum_{k=-\lfloor n_a \rfloor}^{\infty} p(\lfloor n_a \rfloor + k)(\lfloor n_a \rfloor + k) = n_a. \quad \text{(A3)}$$

The second-order correlation function for such states is then found as:

$$g^{(2)} = \sum_{k=-\lfloor n_a \rfloor}^{\infty} (\lfloor n_a \rfloor + k)(\lfloor n_a \rfloor + k - 1)p(\lfloor n_a \rfloor + k)/n_a^2. \quad \text{(A4)}$$

Since n_a is the same for both states (A1) and (A2) when Eq. (A3) is satisfied, it is enough for the comparison of their antibunching to consider the difference of their $n_a^2 g^{(2)}$ (effectively getting rid of the denominator, which simplifies the notations). We call this difference $\Delta G^{(2)}$ and find, from Eqs. (11) and (A4),

$$\begin{aligned}
\Delta G^{(2)} &= \sum_{k=-\lfloor n_a \rfloor}^{\infty} (\lfloor n_a \rfloor + k)(\lfloor n_a \rfloor + k - 1)p(\lfloor n_a \rfloor + k) \\
&\quad - \lfloor n_a \rfloor(\lfloor n_a \rfloor - 1)(\lfloor n_a \rfloor - n_a + 1) \\
&\quad - \lfloor n_a \rfloor(\lfloor n_a \rfloor + 1)(n_a - \lfloor n_a \rfloor) \\
&= \left[\sum_{k \neq \{0,1\}} (\lfloor n_a \rfloor + k)(\lfloor n_a \rfloor + k - 1)p(\lfloor n_a \rfloor + k) \right] \\
&\quad + \lfloor n_a \rfloor(\lfloor n_a \rfloor - 1)[p(\lfloor n_a \rfloor) - \lfloor n_a \rfloor + n_a] \\
&\quad + \lfloor n_a \rfloor(\lfloor n_a \rfloor + 1)[p(\lfloor n_a \rfloor + 1) - (n_a - \lfloor n_a \rfloor)],
\end{aligned}$$

where we have separated the terms $k = 0, 1$ from the sum and rearranged the factors. Now, since $p(\lfloor n_a \rfloor + 1) = 1 - p(\lfloor n_a \rfloor) - \sum_{k \neq \{0,1\}} p(\lfloor n_a \rfloor + k)$ from the probability normalization, we arrive to:

$$\begin{aligned}
\Delta G^{(2)} &= \left[\sum_{k \neq \{0,1\}} (k-1)(2\lfloor n_a \rfloor + k)p(\lfloor n_a \rfloor + k) \right] \\
&\quad - 2\lfloor n_a \rfloor[p(\lfloor n_a \rfloor) - \lfloor n_a \rfloor + n_a - 1]. \quad \text{(A5)}
\end{aligned}$$

On the other hand, from Eq. (A3), we can isolate:

$$p(\lfloor n_a \rfloor) = \lfloor n_a \rfloor - n_a + 1 + \sum_{k \neq \{0,1\}} (k-1)p(\lfloor n_a \rfloor + k), \quad \text{(A6)}$$

which, injected back in Eq. (A5), yields:

$$\Delta G^{(2)} = \sum_{k \neq \{0,1\}} k(k-1)p(\lfloor n_a \rfloor + k). $$

This is the final result since all the terms in the sum are non-negative, so we can conclude that $\Delta G^{(2)} \geq 0$. The inequality is maximized when *all* the probabilities $p(\lfloor n_a \rfloor + k) = 0$ for $k \neq \{0,1\}$, i.e., for the states of type (A1). When n_a is an integer, i.e., $\lfloor n_a \rfloor = n_a$, the maximum antibunching is obtained with the Fock state $|n_a\rangle$. ∎

Proposition. For a given population $n_a \in \mathbb{R}$ and any positive real number δ, there is at least one state such that $\Delta G^{(2)} = \delta$.

Let us consider the set of states with population $n_a = \sum_n np(n)$. We can construct a state ρ_0 with population n_a in the following way:

$$\begin{aligned}
\rho_0 &= p(0)|0\rangle\langle 0| + p(\lfloor n_a \rfloor)|\lfloor n_a \rfloor\rangle\langle\lfloor n_a \rfloor| \\
&\quad + [1 - p(0) - p(\lfloor n_a \rfloor)]|k\rangle\langle k|.
\end{aligned}$$

Imposing the population constraint, we obtain the following condition:

$$p(0) = \left(\frac{k - n_a}{k}\right) - p(\lfloor n_a \rfloor)\left(\frac{k - \lfloor n_a \rfloor}{k}\right),$$

where we have assumed that $\lfloor n_a \rfloor < k \in \mathbb{N}$. The $g^{(2)} = g_*^{(2)} + \delta$ of this state is given by:

$$g^{(2)} n_a^2 = \lfloor n_a \rfloor (\lfloor n_a \rfloor - 1) p(\lfloor n_a \rfloor) + k(k-1)[1 - p(0) - p(\lfloor n_a \rfloor)],$$

where $g_*^{(2)}$ is the minimum $g^{(2)}$ as given in Eq. (11), and from which we can obtain $p(\lfloor n_a \rfloor)$:

$$p(\lfloor n_a \rfloor) = \frac{n_a(k - 1 - n_a g^{(2)})}{\lfloor n_a \rfloor (k - \lfloor n_a \rfloor)}.$$

Only if $\delta > 0$, we can find an integer number $k > \max(n_a g^{(2)}, \lfloor n_a \rfloor)$ such that $0 \leqslant p(\lfloor n_a \rfloor) \leqslant 1$. Considering that this state is not made of two consecutive Fock states, the accessible $g^{(2)}$'s are larger than $g_*^{(2)}$. Of course, when $p(0) = 0$ and $k = \lfloor n_a \rfloor + 1$, ρ_0 is the maximally antibunched state and

$g^{(2)} = g_*^{(2)}$. When $n_a < 1$, $\lfloor n_a \rfloor = 0$, and the procedure above fails. In such case, we can build another state:

$$\rho_1 = p(0)|0\rangle\langle 0| + p(1)|1\rangle\langle 1| + [1 - p(0) - p(1)]|k\rangle\langle k|,$$

such that $n_a = p(1) + k[1 - p(0) - p(1)]$. From this constraint we obtain the following condition:

$$p(1) = \frac{k[1 - p(0)] - n_a}{k - 1}.$$

The $g^{(2)}$ of this state is given by:

$$g^{(2)} n_a^2 = k(k-1)[1 - p(0) - p(1)]$$
$$= k[n_a + p(0) - 1],$$

from which we conclude that:

$$p(0) = \frac{g^{(2)} n_a^2 + k(1 - n_a)}{k}.$$

Again, we can always find an integer $k > 1$, such that $0 \leqslant p(0) \leqslant 1$.

[1] B. E. A. Saleh and M. C. Teich, *Fundamentals of Photonics*, 2nd ed. (Wiley Interscience, Hoboken, NJ, 2007).

[2] J. F. Clauser, Experimental distinction between the quantum and classical field-theoretic predictions for the photoelectric effect, Phys. Rev. D **9**, 853 (1974).

[3] H. J. Kimble, M. Dagenais, and L. Mandel, Photon Antibunching in Resonance Fluorescence, Phys. Rev. Lett. **39**, 691 (1977).

[4] P. Michler *et al.*, A quantum dot single-photon turnstile device, Science **290**, 2282 (2000).

[5] A. J. Shields, Semiconductor quantum light sources, Nat. Photonics **1**, 215 (2007).

[6] M. D. Eisaman, J. Fan, A. Migdall, and S. V. Polyakov, Single-photon sources and detectors, Rev. Sci. Instrum. **82**, 071101 (2011).

[7] A. V. Kuhlmann *et al.*, Transform-limited single photons from a single quantum dot, Nat. Commun. **6**, 8204 (2015).

[8] S. L. Portalupi *et al.*, Bright phonon-tuned single-photon source, Nano Lett. **15**, 6290 (2015).

[9] K. Müller, A. Rundquist, K. A. Fischer, T. Sarmiento, K. G. Lagoudakis, Y. A. Kelaita, C. Sánchez Muñoz, E. del Valle, F. P. Laussy, and J. Vučković, Coherent Generation of Nonclassical Light on Chip Via Detuned Photon Blockade, Phys. Rev. Lett. **114**, 233601 (2015).

[10] X. Ding, Y. He, Z.-C. Duan, N. Gregersen, M.-C. Chen, S. Unsleber, S. Maier, C. Schneider, M. Kamp, S. Höfling, C.-Y. Lu, and J.-W. Pan, On-demand Single Photons with High Extraction Efficiency and Near-Unity Indistinguishability from a Resonantly Driven Quantum Dot in a Micropillar, Phys. Rev. Lett. **116**, 020401 (2016).

[11] N. Somaschi *et al.*, Near-optimal single-photon sources in the solid state, Nat. Photonics **10**, 340 (2016).

[12] C. J. Chunnilall, I. P. Degiovanni, S. Kück, I. Müller, and A. G. Sinclair, Metrology of single-photon sources and detectors: a review, Opt. Eng. **53**, 081910 (2014).

[13] M. Ware and A. Migdall, Single-photon detector characterization using correlated photons: The march from feasibility to metrology, J. Mod. Opt. **51**, 1549 (2004).

[14] M. A. Taylor and W. P. Bowen, Quantum metrology and its application in biology, Phys. Rep. **615**, 1 (2016).

[15] A. Beveratos, R. Brouri, T. Gacoin, A. Villing, J.-P. Poizat, and P. Grangier, Single Photon Quantum Cryptography, Phys. Rev. Lett. **89**, 187901 (2002).

[16] A. Kiraz, M. Atatüre, and A. Imamoğlu, Quantum-dot single-photon sources: Prospects for applications in linear optics quantum-information processing, Phys. Rev. A **69**, 032305 (2004).

[17] V. Tamma and S. Laibacher, Multiboson Correlation Interferometry with Arbitrary Single-photon Pure States, Phys. Rev. Lett. **114**, 243601 (2015).

[18] N. Lambert *et al.*, Quantum biology, Nat. Phys. **9**, 10 (2013).

[19] J. N. Tinsley *et al.*, Direct detection of a single photon by humans, Nat. Commun. **7**, 12172 (2016).

[20] R. H. Hadfield, Single-photon detectors for optical quantum information applications, Nat. Photonics **3**, 696 (2009).

[21] G. Reithmaier *et al.*, On-chip time resolved detection of quantum dot emission using integrated superconducting single photon detectors, Sci. Rep. **3**, 1901 (2013).

[22] M. Kira and S. W. Koch, Quantum-optical spectroscopy of semiconductors, Phys. Rev. A **73**, 013813 (2006).

[23] M. Aßmann and M. Bayer, Nonlinearity sensing via photon-statistics excitation spectroscopy, Phys. Rev. A **84**, 053806 (2011).

[24] M. Aßmann and M. Bayer, Stochastic pumping of a polariton fluid, Phys. Rev. A **91**, 053835 (2015).

[25] S. Mukamel and K. E. Dorfman, Nonlinear fluctuations and dissipation in matter revealed by quantum light, Phys. Rev. A **91**, 053844 (2015).

[26] J. C. López Carreño, C. Sánchez Muñoz, D. Sanvitto, E. del Valle, and F. P. Laussy, Exciting Polaritons with Quantum Light, Phys. Rev. Lett. **115**, 196402 (2015).

[27] E. del Valle, A. Gonzalez-Tudela, F. P. Laussy, C. Tejedor, and M. J. Hartmann, Theory of Frequency-filtered and Time-resolved n-photon Correlations, Phys. Rev. Lett. **109**, 183601 (2012).

[28] E. del Valle, Distilling one, two and entangled pairs of photons from a quantum dot with cavity QED effects and spectral filtering, New J. Phys. **15**, 025019 (2013).

[29] A. González-Tudela, F. P. Laussy, C. Tejedor, M. J. Hartmann, and E. del Valle, Two-photon spectra of quantum emitters, New J. Phys. **15**, 033036 (2013).

[30] C. Sánchez Muñoz, E. del Valle, C. Tejedor, and F. Laussy, Violation of classical inequalities by photon frequency filtering, Phys. Rev. A **90**, 052111 (2014).

[31] A. González-Tudela, E. del Valle, and F. P. Laussy, Optimization of photon correlations by frequency filtering, Phys. Rev. A **91**, 043807 (2015).

[32] K. Kamide, S. Iwamoto, and Y. Arakawa, Eigenvalue decomposition method for photon statistics of frequency-filtered fields and its application to quantum dot emitters, Phys. Rev. A **92**, 033833 (2015).

[33] M. Peiris, B. Petrak, K. Konthasinghe, Y. Yu, Z. C. Niu, and A. Muller, Two-color photon correlations of the light scattered by a quantum dot, Phys. Rev. B **91**, 195125 (2015).

[34] C. W. Gardiner, Driving a Quantum System with the Output Field from Another Driven Quantum System, Phys. Rev. Lett. **70**, 2269 (1993).

[35] H. J. Carmichael, Quantum Trajectory Theory for Cascaded Open Systems, Phys. Rev. Lett. **70**, 2273 (1993).

[36] D. F. Walls, Squeezed states of light, Nature (London) **306**, 141 (1983).

[37] D. M. Toyli, A. W. Eddins, S. Boutin, S. Puri, D. Hover, V. Bolkhovsky, W. D. Oliver, A. Blais, and I. Siddiqi, Resonance Fluorescence from an Artificial Atom in Squeezed Vacuum, Phys. Rev. X **6**, 031004 (2016).

[38] M. Kolobov and I. Sokolov, Interference of a physical field and of the vacuum fluctuations at the output of a light source, Opt. Spectrosk. **62**, 112 (1989).

[39] G. W. Gardiner and P. Zoller, *Quantum Noise*, 2nd ed. (Springer, Berlin, 2000).

[40] C. W. Gardiner and A. S. Parkins, Driving atoms with light of arbitrary statistics, Phys. Rev. A **50**, 1792 (1994).

[41] J. I. Cirac, P. Zoller, H. J. Kimble, and H. Mabuchi, Quantum State Transfer and Entanglement Distribution Among Distant Nodes in a Quantum Network, Phys. Rev. Lett. **78**, 3221 (1997).

[42] W. S. Smyth and S. Swain, Complete quenching of fluorescence from a two-level atom driven by a weak, narrow-band, nonclassical light field, Phys. Rev. A **59**, R2579(R) (1999).

[43] A. Messikh, R. Tanaś, and Z. Ficek, Response of a two-level atom to a narrow-bandwidth squeezed-vacuum excitation, Phys. Rev. A **61**, 033811 (2000).

[44] M. Grundmann, O. Stier, and D. Bimberg, InAs/GaAs pyramidal quantum dots: Strain distribution, optical phonons, and electronic structure, Phys. Rev. B **52**, 11969 (1995).

[45] J. Petersen, J. Volz, and A. Rauschenbeutel, Chiral nanophotonic waveguide interface based on spin-orbit interaction of light, Science **346**, 67 (2014).

[46] C. Gonzalez-Ballestero, A. Gonzalez-Tudela, F. J. Garcia-Vidal, and E. Moreno, Chiral route to spontaneous entanglement generation, Phys. Rev. B **92**, 155304 (2015).

[47] H. Pichler, T. Ramos, A. J. Daley, and P. Zoller, Quantum optics of chiral spin networks, Phys. Rev. A **91**, 042116 (2015).

[48] R. J. Coles *et al.*, Chirality of nanophotonic waveguide with embedded quantum emitter for unidirectional spin transfer, Nat. Commun. **7**, 11183 (2016).

[49] S. Mahmoodian, P. Lodahl, and A. S. Sorensen, Quantum networks with chiral light-matter interaction in waveguides, arXiv:1602.07054.

[50] P.-O. Guimond, H. Pichler, A. Rauschenbeutel, and P. Zoller, Chiral quantum optics with V-level atoms and coherent quantum feedback, Phys. Rev. A **94**, 033829 (2016).

[51] P. Lodahl *et al.*, Chiral quantum optics, arXiv:1608.00446.

[52] C. Gonzalez-Ballestero, E. Moreno, F. J. García-Vidal, and A. Gonzalez-Tudela, Non-reciprocal few-photon devices based on chiral waveguide-emitter couplings, arXiv:1608.04928.

[53] J. C. López Carreño, C. Sánchez Muñoz, E. del Valle, and F. P. Laussy, Excitation with quantum light. II. Exciting a two-level system, Phys. Rev. A **94**, 063826 (2016).

[54] F. P. Laussy, I. A. Shelykh, G. Malpuech, and A. Kavokin, Effects of Bose–Einstein condensation of exciton polaritons in microcavities on the polarization of emitted light, Phys. Rev. B **73**, 035315 (2006).

[55] A. I. Lvovsky, *Fundamentals of Photonics and Physics* (Wiley, Hoboken, NJ, 2015), Chap. 5.

[56] S. Haroche and J.-M. Raimond, *Exploring the Quantum: Atoms, Cavities, and Photons* (Oxford University Press, Oxford, 2006).

[57] D. Stoler, B. Saleh, and M. Teich, Binomial states of the quantized radiation field, Opt. Acta **32**, 345 (1985).

[58] M. M. Nieto, Displaced and squeezed number states, Phys. Lett. A **229**, 135 (1997).

[59] S. Dong, T. Huang, Y. Liu, J. Wang, G. Zhang, L. Xiao, and S. Jia, Fast recognition of single molecules based on single-event photon statistics, Phys. Rev. A **76**, 063820 (2007).

[60] V. B. Verma *et al.*, Photon antibunching from a single lithographically defined InGaAs/GaAs quantum dot, Opt. Express **19**, 4182 (2011).

[61] G. D. Martino *et al.*, Quantum statistics of surface plasmon polaritons in metallic stripe waveguides, Nano Lett. **12**, 2504 (2012).

[62] M. Leifgen *et al.*, Evaluation of nitrogen- and silicon-vacancy defect centres as single photon sources in quantum key distribution, New J. Phys. **16**, 023021 (2014).

[63] E. Zubizarreta Casalengua, J. C. López Carreño, E. del Valle, and F. P. Laussy, Structure of the harmonic oscillator Hilbert space, arXiv:1607.03976.

[64] H. Flayac and V. Savona, Heralded Preparation and Readout of Entangled Phonons in a Photonic Crystal Cavity, Phys. Rev. Lett. **113**, 143603 (2014).

[65] E. del Valle and F. P. Laussy, Regimes of strong light-matter coupling under incoherent excitation, Phys. Rev. A **84**, 043816 (2011).

[66] C. Sánchez Muñoz *et al.*, Emitters of *N*-photon bundles, Nat. Photonics **8**, 550 (2014).